Journal of Materials Chemistry C

Accepted Manuscript

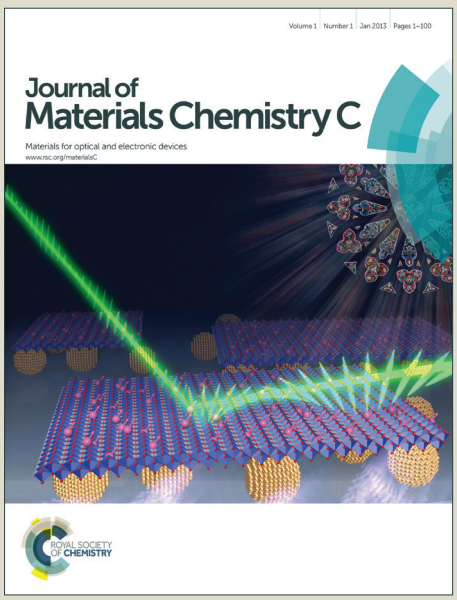

ROYAL SOCIETY OF CHEMISTRY

www.rsc.org/materialsC

Journal of
Materials Chemistry C

PAPER

Effect of functionalized π-bridge on porphyrin sensitizers for dye-sensitized solar cells: An in-depth analysis of electronic structure, spectrum, excitation, and intramolecular electron transfer†

Xiaoqing Lu,*[‡] Yang Shao,[‡] Shuxian Wei, Zigang Zhao, Ke Li, Chen Guo, Weili Wang, Mingmin Zhang and Wenyue Guo*

Received 00th July 2015,
Accepted 00th July 2015

DOI: 10.1039/x0xx00000x

www.rsc.org/MaterialsC

A series of porphyrin sensitizers for dye-sensitized solar cells (DSSCs) have been systematically investigated by density functional theory (DFT) and time-dependent DFT (TD-DFT) in tetrahydrofuran (THF) solution. Effects of π-bridge length, heteroaromatic unit, longitudinal conjugation, and relative position of functionalized groups on the optical and electrical properties are elucidated by analyzing the geometry, electronic structure, electron excitation, spectrum, photo-induced intramolecular electron transfer (IET), and light-harvesting efficiency (LHE). Our results show that the increase in π-bridge length by adding phenyl group distances the electron distribution of LUMO away from anchoring group and sharply decreases the effective electron excitation at the long wavelength region. The introduction of heteroaromatics in π-bridge, especially electron-deficient units, stabilizes LUMO levels and improves the light-harvesting capability and donor-to-acceptor IET characteristic significantly. The extension of longitudinal π-conjugation in π-bridge broadens the B band and slightly strengthens and redshifts the Q band but results in undesired orbital overlap. Repositioning Phenyl/Thiophene group away from carboxylic acid enlarges the energy gap but yield more effective long-range IET processes with more electron, longer distance, lower orbital overlap, and moderate transfer rate. Our results highlight the significant effect of functionalized π-bridge on porphyrin sensitizers, and provide a fresh insight into the design and screening of sensitizers for DSSCs.

1. Introduction

Dye-sensitized solar cells (DSSCs), as a potential cost-efficient photoelectric conversion device for green energy resource, have attracted wide attention over the past two decades [1-6]. The sensitizer, which is usually adsorbed on a semiconductor electrode, plays a crucial role in light harvesting by pumping electrons from the lower ground state to higher excited state energy levels, and thus generating electric potential differences. High-performance DSSCs can be achieved by suitable molecular engineering of sensitizers [7-10]. At present, Ru(II)-based sensitizers exhibit high photon-to-electron power conversion efficiencies (PCEs) over 12% [4]; however, the high cost, limited availability and environmental issues associated with ruthenium constrain the extensive application of such sensitizers [11,12]. Comparatively, organic sensitizers are advantageous given their low cost, high molar extinction coefficient, good flexibility, and environmental compatibility [5,13-15]. Among these sensitizers, porphyrin chromophores are perceived to be among the most promising candidates for panchromatic absorption due to the outstanding capability to capture solar energy in the visible region, as well as their structural similarity to the chlorophylls in natural photosynthetic systems [12,16,17].

Porphyrin-based sensitizers typically adopt the structure of donor-π-acceptor (D-π-A), which facilitates molecular tailoring and enriches the diversity of porphyrin sensitizers [18-21]. DSSC performance has progressed remarkably with such sensitizers via appropriate molecular engineering on donor [8,22-28], π-bridge [10,16,17,29-32], and acceptor [18,20,33,34] subunits. The π-bridge, affecting the electronic coupling between the Zn-porphyrin donor and the anchoring acceptor, is crucial to the charge separation and electron injection after photoexcitation. Yeh and Diau *et al*. synthesized porphyrins **YD11–YD13** that bear benzene, naphthalene, and anthracene rings with extra longitudinal conjugation as π-bridges. These researchers obtained an overall PCE (η = 6.7%) for **YD12** relative to that for N719 (η = 6.1%) [16]. Integrating alkyl-thiophene with benzothiadiazole (BTD), 2,3,5,6-tetrafluorophenylethynyl, diketopyrrolopyrrole, and thiophene (Th) into the π-bridges in porphyrin sensitizers generated PCEs in the range of 4.6% – 8.7% [13, 36-40]. In early 2014, Grätzel *et al*. broadened the absorption spectra of Zn-porphyrin sensitizers to fill the valley between the Soret (B) and Q bands by inserting electron-deficient 2,1,3-BTD as the π-bridge in **GY50**. These researchers achieved a high PCE of 12.75%, thereby highlighting the effect of the phenyl (Ph) group on efficient

College of Science, China University of Petroleum, Qingdao, Shandong 266580, People's Republic of China. E-mail: luxq@upc.edu.cn and wyguo@upc.edu.cn; Fax: +86 532 8698 3363; Tel: +86 532 8698 3372.

† Electronic Supplementary Information (ESI) available: The simulated absorption spectra of **SM315** and **SM371** obtained with four functionals; The first three frontier molecular orbitals and optical transitions between 350.0 and 800.0 nm of other eight porphyrin sensitizers; The first three energy levels of all porphyrin sensitizers. See DOI: 10.1039/x0xx00000x

‡ These authors have made an equal contribution to this work.

prohibition of electron recombination [10]. Very recently, a porphyrin-sensitized solar cell with an overall PCE of 13.0% was generated with the sensitizer **SM315** [40], in which one more Ph group was introduced into the π-bridge relative to **SM371**. In short, extensive experimental efforts were devoted to boost the PCEs of DSSCs. However, the intrinsic mechanisms of the effect of π-bridges on the photon-to-electron performance of porphyrin sensitizers, including the electronic structure, electron excitation and absorption spectral, photo-induced intramolecular electron transfer rate, transfered distance and quantity, and recombination, etc., remain unclear and urgently need to be addressed.

In the current work, a series of porphyrin sensitizers are designed on the basis of reference sensitizers **SM315** and **SM371** with a prototypical D-π-A structure in tetrahydrofuran (THF) solution by DFT and TD-DFT approach. The effects of π-bridges with different functionalized groups on the performance of porphyrin sensitizers are evaluated. Molecular geometry, electronic structure, the characteristics of absorption spectra, electron transfer process, light-harvesting efficiency (LHE), and photo-induced IET performance are analyzed in detail. This work provides not only a comprehensive overview of the general rule regarding functionalized π-bridge groups on porphyrin sensitizers, but also an effective strategy for the design and screening of high-performance porphyrin sensitizers for DSSCs.

2. Computational details

The geometrical optimizations for all porphyrin sensitizers were carried out by using the B3LYP exchange correlation functional [41,42] in conjunction with the 6-31G(d) [43] basis set in THF solution. The frequency analysis was then performed to confirm the nature of each ground-state geometries at the same levels. The standard hybrid functional B3LYP, long-range corrected functional Cam-B3LYP [44-46] and PBE0 [47,48], and the meta-hybrid xc-functional M06 (27% of exact exchange) [49] were used to evaluate the optical properties and photo-induced IET properties. The vertical excitation energy was efficiently calculated by the corresponding TD-DFT methods [50-52]. The first 30 excited singlet states were taken into account in the calculations of the absorption spectra. Considering that the THF solvent is used in the relevant experimental absorption measurements, the real THF environment for porphyrin sensitizers were simulated by the nonequilibrium [53] implementation of the conductor-like polarizable continuum model (C-PCM) [54-56]. All calculations were accomplished with the Gaussian 09 program package [57].

According to Marcus theory, the IET rate k_{ET} is determined by the reorganization energy (λ), the electronic coupling constant (V_{ab}), and the standard Gibbs free energy change (ΔG°) [58]. The IET rate k_{ET} is given as,

$$k_{ET} = \frac{1}{\hbar}|V_{ab}|^2\sqrt{\frac{\pi}{\lambda k_B T}}\exp\left(-\frac{(\Delta G^\circ + \lambda)^2}{4\lambda k_B T}\right) \quad (1)$$

where $\hbar$, k_B, and T represents the Planck constant, Boltzmann constant, and temperature, respectively. The reorganization energy reflects the geometry relaxation in the involved donor and acceptor when their electronic state changes; the electronic coupling reflects the overlap of the wave functions between two charge-localized states [59]. As a self-exchange process, the standard Gibbs free energy change before and after the IET process is considered as zero (ΔG° = 0) [60,61]. The inner-sphere reorganization energy (λ_v) [60,62,63] describes the geometry changes of donor and acceptor in electron transfer process [64,65], which is evaluated by Nelson's four-point method [62,66],

$$\lambda_v = E_+^* - E_+ + E^* - E \quad (2)$$

where E_+^* and E_+ is the energy of the cationic donor (D^+) at the neutral-state and optimal cationic-state geometry, and accordingly, E^* and E is the energy of the neutral acceptor (A) at the cationic-state and optimized neutral-state geometry, respectively [63,67,68]. In the calculations, the sensitizers are not explicitly splitted into D^+ and A but considered as a whole [60,69,70]. The generalized Mulliken−Hush (GMH) method connecting with the dipole moments and vertical transition energy is employed to estimate the value of electronic coupling and all data can be read from the Gaussian output files [69,71],

$$V_{ab} = \frac{\mu_{ab}\Delta E_{ab}}{\sqrt{\Delta\mu_{ab}^2 + 4\mu_{ab}^2}} \quad (3)$$

where μ_{ab}, ΔE_{ab}, and $\Delta\mu_{ab}$ is the transition dipole moment, the vertical excitation energy, and the dipole moment difference between the initial and final adiabatic states, respectively.

3. Results and discussion

In the following, the accuracy of the chosen computational methods is first calibrated. Then, the molecular geometry of porphyrin sensitizers, the molecular orbitals and electronic structure, the properties of electron excitation and absorption spectra are analyzed. Next, the relation between structural optimization and LHE performance is discussed. Finally, the photo-induced IET properties are elucidated.

3.1 Calibration

To calibrate the accuracy of the chosen methods, the results calculated with different functionals are compared with both experimental and theoretical data [40]. Fig. S1 (ESI†) presents the simulated UV-Vis absorption spectra of sensitizers **SM315** and **SM371** [40] obtained with four functionals in THF solution. The spectra obtained with the CAM-B3LYP functional leads to a blue shift throughout the spectral coverage. The absorption peaks are detected at ~380/413/546/614 nm for **SM315** and at ~405/599 nm for **SM371**; these values are approximately 40 nm smaller than the reference experimental values of 454/668 nm and 447/646 nm, respectively [40]. Given the B3LYP, PBE0, and M06 functionals, the calculated locations of the absorption peak are at ~431/763, ~417/709 and ~418/699 nm for **SM315** and at ~433/699, ~424/662 and ~431/658 nm for **SM371**. Obviously, the spectral data obtained with M06 match considerably better with the experimental values than those obtained with other functionals.

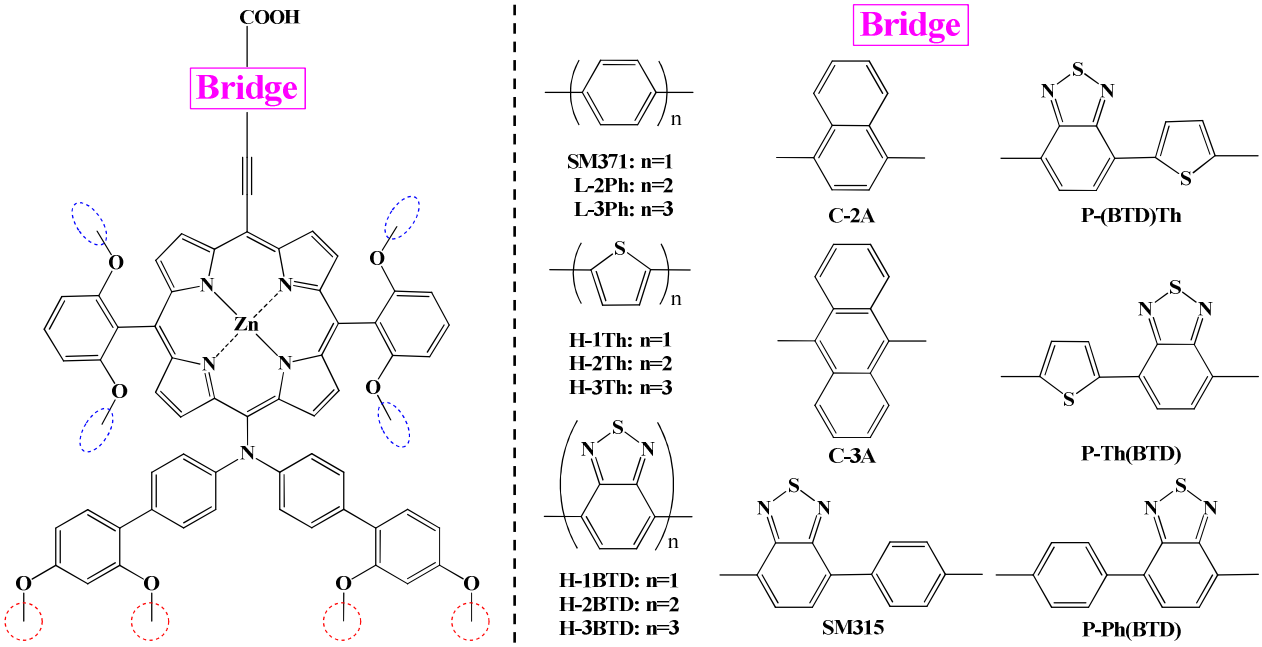

Fig. 1 Sketch of chemical structures of porphyrin sensitizers. The $C_6H_{13}^+$ and $C_8H_{17}^+$ groups are replaced by methyl groups marked with red dash-lined circles and blue dash-lined ellipses.

On the other hand, the first vertical excitation energies of **SM315** and **SM371** as calculated with four functionals are ordered as follows: 1.62 eV (B3LYP) < 1.74 eV (PBE0) < 1.77 eV (M06) < 2.02 eV (CAM-B3LYP) and 1.78 eV (B3LYP) < 1.87 eV (PBE0) < 1.88 eV (M06) < 2.07 eV (CAM-B3LYP). The M06 functional provides the closest results on the crucial electron excitations given the experimental values of 1.86 eV for **SM315** and 1.92 eV for **SM371**, respectively [40]. Considering both absorption spectra and electron excitations, the agreement of the M06 results with the experimental data demonstrates the reliability of the method and the level of theory. Therefore, the results of M06/6-31G(d) are referenced in the discussion unless otherwise stated.

3.2 Molecular geometry

The molecular geometries of porphyrin sensitizers are illustrated in Fig. 1. Given the structure of reference sensitizers **SM315** and **SM371**, each newly designed porphyrin sensitizer is constructed with a Zn-porphyrin core, a bulky bis(2',4'-bis(hexyloxy)-[1,1'-biphenyl]-4-yl)amine as a donor, and carboxylic acid as an anchoring group [40]. These components are linked by various combinations of Ph, Th, acenes and BTD as a π-bridge. To balance accuracy and efficiency, the long alkoxy chains of hexyloxy and octyloxy in porphyrin sensitizers are replaced by the methoxy groups at the *ortho* and *para* positions of each *meso*-phenyl ring and the bis(2',4'-bis(hexyloxy)-[1,1'-biphenyl]-4-yl)amine donor. These substitutions are previously proven to have minor effect on the optical properties [14,46].

The structural design is based on the following considerations: (1) adding 1 – 2 more π-conjugated Ph units in the π-bridge subunit [32,72] of **SM371** (labeled as **L-2Ph** and **L-3Ph**) to estimate the effect of π-bridge length; (2) introducing 1 – 3 electron-rich Th and electron-deficient BTD as π-bridge linkers (labeled as **H-1Th** – **H-3Th** and **H-1BTD** – **H-3BTD**, respectively) [10,12,29,30] to evaluate the effect of heteroaromatics as well as the π-bridge length; (3) substituting acene for Ph linkers (**SM371** → **C-1A**, **C-2A**) to clarify the longitudinal π-conjugation effect [16,17]; and (4) replacing a Ph unit with Th (**SM315** → **P-(BTD)Th**) and rearranging the order of units in a π-bridge subunit (**SM315** → **P-Ph(BTD)** and **P-(BTD)Th** → **P-Th(BTD)**) to determine the position effect [19].

3.3 Molecular orbital and electronic structure

Crucial electron excitations mainly occur from the highest occupied molecular orbitals (HOMOs) to the lowest unoccupied molecular orbitals (LUMOs); therefore, efficient charge-separated states must be formed with the HOMOs localized on the donor subunit and the LUMOs on the acceptor subunit [7,46]. Fig. 2 shows the first three molecular orbital energies and the HOMO-LUMO gaps of porphyrin sensitizers. In consideration of the similarities, **L-2Ph**, **H-2Th**, **H-2BTD**, **C-2A**, and **P-(BTD)Th** are chosen to exhibit the electron contributions of the first three highest HOMOs and of the lowest LUMOs together with **SM371** and **SM315**, as depicted in Fig. 3. The results of other sensitizers are presented in Fig. S2 (ESI†), and Table S1 (ESI†) lists the corresponding energy levels of porphyrin sensitizers. Seen from Fig. 3, all of the electron distributions in HOMO-2 of porphyrin sensitizers originate from the Zn-porphyrin core, and those in the HOMO-1 and HOMO mainly originate from the bulky bis(2',4'-bis(hexyloxy)-[1,1'-biphenyl]-4-yl)amine group[40] and the Zn-porphyrin core. The alteration of π-bridge linkers exerts little effect on the HOMOs (except for **P-Ph(BTD)**), in good agreement with the results obtained by Grätzel *et. al* [40]. Therefore,

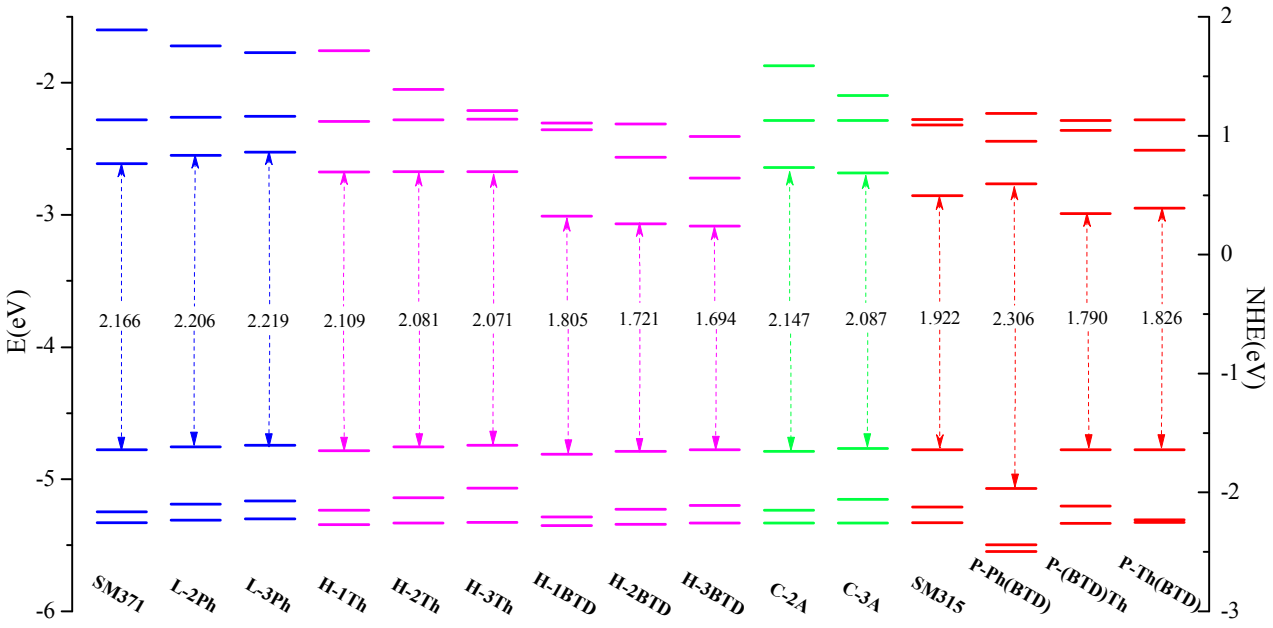

Fig. 2 The first three energy levels and HOMO-LUMO gaps of porphyrin sensitizers.

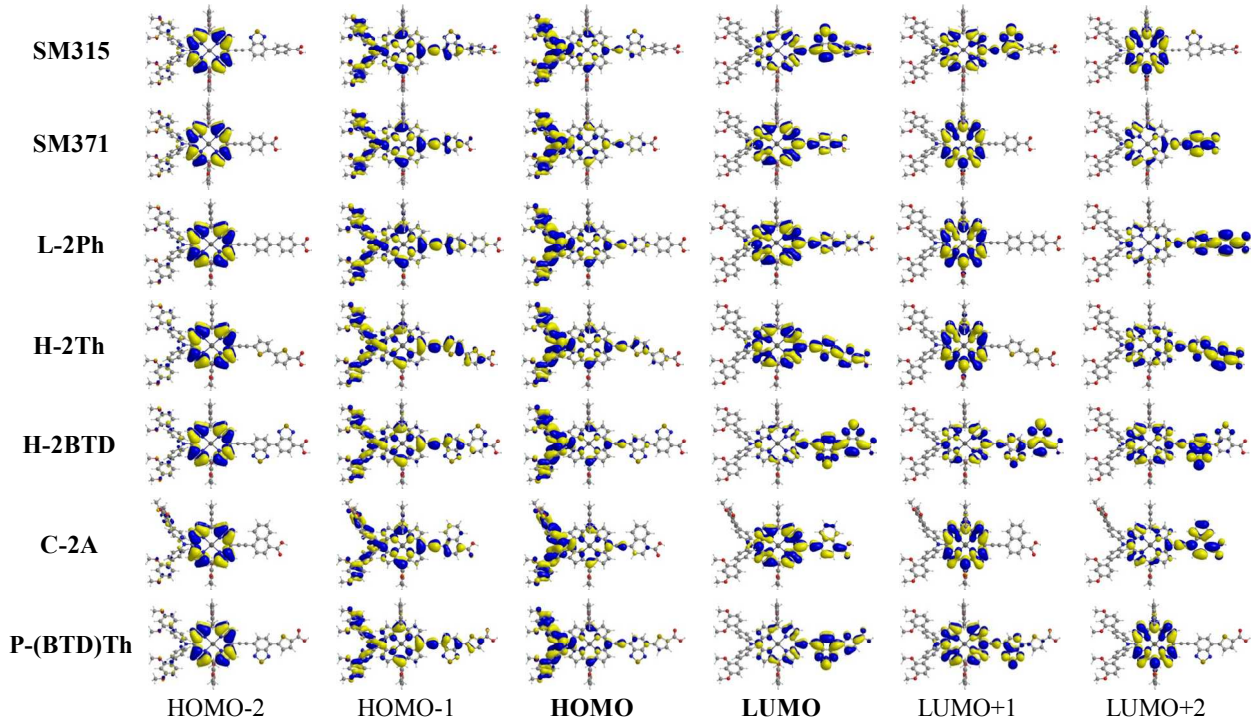

Fig. 3 The first three frontier molecular orbitals of **SM315**, **SM371**, **L-2Ph**, **H-2Th**, **H-2BTD**, **C-2A**, and **P-(BTD)Th**. Isodensity contour = 0.02.

much attention is paid to the changes in electron contribution to LUMOs as a result of π-bridge modification.

For Ph-bridged porphyrin sensitizers **SM371**, **L-2Ph** and **L-3Ph**, as indicated in Figs. 3 and S2 (ESI†), the electron distribution in LUMO+2 is primarily observed on the functionalized bridges and the associated carboxylic acid anchoring group. The distribution atthese locations is conducive to the electron injection from the porphyrin sensitizers to the semiconductor surface. The LUMO+1 of these three sensitizers is completely derived from the Zn-porphyrin core, indicating that LUMO+1 cannot generate an effective charge-separated state but aggravate electron recombination. For LUMO, with an increase in bridge length (**SM371** → **L-2Ph** → **L-3Ph**), the electron distribution is gradually distanced from the anchoring group. Therefore, charge separation efficiency decreases sharply. In

addition, the HOMO-LUMO gap increases with an increase of Ph groups in π-bridge linker as a result of the rise in LUMO energy level, as shown in Fig. 2. A long π-bridge length increases the energy gap; thus, more excitation energy is required to form a charge-separated state from **SM371** (2.166 eV) to **L-2Ph** (2.206 eV) and **L-3Ph** (2.219 eV). This agrees well with the previous findings for phenylacetylene-bridged porphyrin sensitizers [32].

Substituting Ph with 1 – 3 electron-rich Th and electron-deficient BTD as π-bridge linkers (**SM371** → **H-1Th** – **H-3Th** and **H-1BTD** – **H-3BTD**) lowers LUMO levels considerably and thus reduces energy gaps, similar to the theoretical results obtained for pyrene-conjugated porphyrin sensitizers **LW17** and **LW18** [12]. The energy gap decreases in the following sequence for Th- and BTD-bridged porhphyrin sensitizers: 2.109 eV (**H-1Th**) > 2.081 eV (**H-2Th**) > 2.071 eV (**H-3Th**) and 1.805 eV (**H-1BTD**) > 1.721 eV (**H-2BTD**) > 1.694 eV (**H-3BTD**), respectively. The shapes of the first three LUMOs of **H-1Th** – **H-3Th** are similar to that of **SM371**, as shown in Figs. 3 and S2 (ESI†). Unlike **SM371** and **H-1Th** – **H-3Th**, the electron distribution of LUMO and LUMO+1 in **H-1BTD** – **H-3BTD** is mainly observed on the π-bridge and the anchoring group. The electron distribution of LUMO+2 locates gradually close to the carboxylic acid group from **H-1BTD** to **H-3BTD**. Changes in both energy gap and electron distribution originate from the difference in electronic characteristics between Ph and Th/BTD groups in a π-bridge. These changes facilitate electron excitation and charge separation, and efficient electron injection into the conduction band (CB) of a semiconductor.

Extending the longitudinal π-conjugation with naphthalene and anthracene (**SM371** → **C-2A**, **C-3A**) stabilizes LUMO levels and reduces the energy gap from 2.166 to 2.147 and 2.087 eV, as with the acene-modified porphyrins **YD11** – **YD13** and **LAC-1** – **LAC-5** [16,17]. The electronic contributions of LUMO and LUMO+2 are broadened to naphthalene and anthracene with the same orbital compositions (Zn-porphyrin core and anchoring group) as those in **SM371**. For LUMO+1 in acene-bridged porphyrin sensitizers, the charge separation efficiency would sharply drops since no excited electron can efficiently reach the carboxylic acid.

When the Ph group is repositioned at a distance from carboxylic acid, **SM315** → **P-Ph(BTD)**, not only does LUMO level increases but HOMO level stabilizes as well. Thus, the energy gap is enlarged to 2.306 eV. A similar trend is observed when the electron-rich Th is repositioned at a distance from the carboxylic acid, **P-(BTD)Th** → **P-Th(BTD)**. Comparing with **SM315**, inserting Th reduces the energy gaps of **P-Th(BTD)** and **P-(BTD)Th** to 1.826 and 1.790 eV, whether or not Th is close to the carboxylic acid. Charge separation efficiency would be improved with LUMO but not with LUMO+1 and LUMO+2 as arriving orbitals, according to the electronic distribution in **P-(BTD)Th** and **P-Th(BTD)**.

To sum up, most of the optimized porphyrin sensitizers with fine adjustments on the π-bridge exhibit suitable electronic distributions and energy levels relative to **SM315** and **SM371**. Therefore, it is believed to match well with the CB of semiconductor and the redox potential of electrolyte, especially the $Co^{II/III}$ tris(bipyridyl) electrolyte [40].

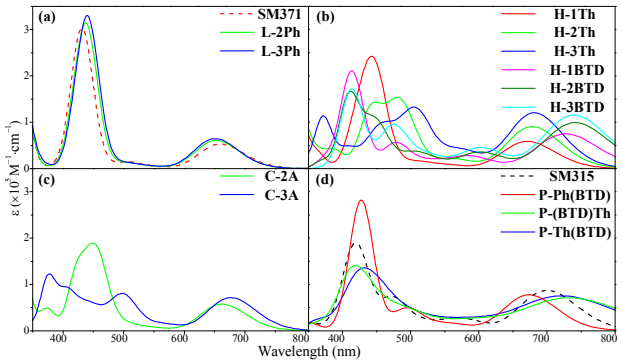

Fig. 4 Simulated absorption spectra of the (a) phenyl-bridged, (b) thiophene-bridged, (c) BTD-bridged porphyrin sensitizers, and (d) **SM315**, **P-Ph(BTD)**, **P-(BTD)Th** and **P-Th(BTD)**.

3.4 Electron excitations and absorption spectra

Table 1 lists the excitation energies, oscillator strengths, and relative orbital contributions of the optical transitions between 350 and 800 nm for the selected sensitizers **L-2Ph**, **H-2Th**, **H-2BTD**, **C-2A**, and **P-(BTD)Th** in THF solution. Electron excitations of other sensitizers are listed in Table S2 (ESI†). The absorption spectra simulated at the M06/6-31G(d) level are presented in Fig. 4.

The absorption spectra of Ph-bridged porphyrin sensitizers exhibit a red-shifted trend for the B band and a blue-shifted trend for the Q band with the increase in the number of Ph groups from **SM371** (431.03/657.89 nm) to **L-2Ph** (436.68/653.59 nm) and **L-3Ph** (440.53/649.35 nm), as indicated in Fig. 4a. The blue-shifted trend for the Q band corresponds to the enlarged HOMO-LUMO gap and indicates a decrease in the spectral coverage from **SM371** to **L-2Ph** and **L-3Ph**. Seen from Table 1, the effective transition of HOMO → LUMO+2 (80%) for **L-2Ph** is found at 399.6 nm with f = 0.036, and a similar transition occurs at 355.3 nm for **L-3Ph**. Unfortunately, the transitions from HOMO to LUMO for **L-2Ph** at 652.9 nm with f = 0.559 and for **L-3Ph** at 651.2 nm with f = 0.593 are ineffective for charge separation according to the frontier molecular orbital analysis. For **SM371**, the band centered at ~660 nm is generated from the transition HOMO → LUMO (91%) with f = 0.487 (Table S2 †), showing main ligand-to-ligand electron transfer (LLET) via the effective charge-separated states. These indicate the negative effect of π-bridge length on photo-to-electron conversion in Ph-bridged porphyrin sensitizers.

Substituting the Ph group with electron-rich Th results in the redshift of spectral peaks to 442.48/671.14, 480.77/680.27, and 505.05/680.27 nm for **H-1Th**, **H-2Th**, and **H-3Th** relative to those of **SM371**, as shown in Fig. 4b. When Th number increases, the B band intensity weakens while the Q band intensity strengthens gradually. The similar trend in spectral intensity is observed with the increase in BTD number, and the Q band peak is redshifted to 724.6, 740.7, and 740.7 nm for **H-1BTD** – **H-3BTD** relative to that at 700.2 nm for **SM315**. The Q band is predominantly produced through the HOMO → LUMO transition for **H-2Th** at 678.7 nm with f = 0.835 and for **H-2BTD** at 741.3 nm with f = 0.913, as indicated in Table 1. For **H-3BTD**, the band centered at ~739 nm originats from effective

Table 1. Selected excitation energies (E, nm), oscillator strengths (*f*), and relative orbital contributions for the optical transitions between 350 and 800 nm of **L-2Ph**, **H-2Th**, **H-2BTD**, **C-2A**, and **P-(BTD)Th**.

E	*f*	Compositions[a]	E	*f*	Compositions	E	*f*	Compositions	E	*f*	Compositions	E	*f*	Compositions
		L-2Ph			H-2→L(10%)	537.8	0.097	H→L+2(49%)	387.9	0.019	H-3→L+2(94%)	378.4	0.011	H-8→L(54%)
652.9	0.559	H→L(90%)	445.3	0.430	H-3→L(22%)			H-2→L(42%)	372.0	0.121	H-4→L+1(42%)			H-7→L(32%)
543.9	0.035	H-1→L(77%)			H-1→L+1(19%)	512.6	0.077	H→L+3(50%)			H-7→L+1(32%)	371.2	0.394	H-4→L+2(72%)
		H-2→L+1(16%)			H→L+2(18%)			H→L+1(21%)	368.8	0.011	H-3→L+3(90%)	351.8	0.034	H-3→L+2(95%)
501.8	0.110	H-1→L+1(39%)			H-2→L(15%)			H-1→L+3(14%)			**C-2A**			**P-(BTD)Th**
		H→L+1(34%)	434.9	0.366	H-3→L(61%)			H-2→L+2(11%)	677.0	0.657	H→L (90%)	735.4	0.961	H→L(88%)
		H-2→L(26%)			H-1→L+1(20%)	502.2	0.207	H-1→L+1(49%)	565.5	0.132	H-1→L (86%)	600.6	0.296	H-1→L(85%)
441.6	2.359	H-2→L+1(58%)			H-2→L(10%)			H→L+3(19%)	508.1	0.125	H→L+1(37%)	531.3	0.129	H→L+2(50%)
		H-1→L(16%)	406.9	0.025	H-1→L+2(57%)			H-2→L+2(14%)			H-1→L+1(32%)			H-2→L(40%)
431.5	0.216	H-3→L(63%)			H-4→L(32%)	490.0	0.022	H-1→L+2(43%)			H-2→L(28%)	491.8	0.458	H-1→L+1(44%)
		H-1→L+1(18%)	391.6	0.093	H-2→L+2(43%)			H-2→L+1(28%)	500.2	0.544	H→L+2(43%)			H-2→L+2(26%)
		H-2→L(17%)			H-3→L+1(19%)			H→L+2(13%)			H-2→L+1(30%)			H→L+1(12%)
418.8	0.838	H-1→L+1(36%)	391.2	0.162	H-2→L+2(42%)	478.1	0.011	H-3→L(94%)			H-1→L+2(10%)	471.4	0.013	H-3→L(95%)
		H-3→L(35%)			H-3→L+1(23%)	451.4	0.753	H-1→L+1(26%)			H-4→L(10%)	449.7	0.507	H-4→L(50%)
		H-2→L(22%)	383.1	0.038	H-7→L(22%)			H-7→L(23%)	473.3	0.160	H-4→L(49%)			H-1→L+1(24%)
399.6	0.036	H→L+2(80%)			H-4→L(20%)			H-4→L(17%)			H→L+2(36%)			H-7→L(15%)
355.2	0.062	H-9→L(40%)			H-1→L+2(12%)			H-2→L+2(16%)	449.9	0.277	H-1→L+1(45%)	417.8	0.063	H-6→L(87%)
		H-7→L(23%)	380.1	0.028	H-8→L(71%)	438.3	0.108	H-1→L+3(52%)			H-2→L(28%)	416.1	0.752	H-2→L+2(21%)
		H-1→L+2(17%)			H-7→L(11%)			H-4→L(17%)			H-3→L(14%)			H-2→L+1(15%)
352.2	0.031	H-2→L+2(81%)	371.9	0.108	H-7→L(53%)			H-7→L(12%)	438.9	438.9	H-3→L(82%)			H-1→L+2(13%)
		H-2Th			H-8→L(19%)	434.7	0.133	H-2→L+1(51%)	427.6	0.225	H-1→L+2(54%)			H-4→L(11%)
678.7	0.835	H→L(90%)	362.3	0.116	H-4→L+1(31%)			H-2→L+3(34%)			H-4→L(19%)	415.4	0.854	H-2→L+1(29%)
563.6	0.184	H-1→L(86%)			H-8→L+1(19%)			H-1→L+2(13%)			H→L+2(13%)			H-1→L+2(25%)
506.6	0.123	H-1→L+1(38%)	359.6	0.017	H-8→L+1(60%)	413.1	0.580	H-2→L+3(42%)	410.1	0.138	H-2→L+2(67%)			H-2→L+2(12%)
		H→L+1(34%)			H-4→L+1(10%)			H-1→L+2(26%)			H-4→L+1(20%)	401.6	0.010	H-7→L(48%)
		H-2→L(26%)	354.9	0.168	H-4→L+1(35%)			H-3→L+1(15%)	405.1	0.553	H-2→L+1(34%)			H-8→L(21%)
484.1	1.231	H→L+2(43%)			**H-2BTD**	410.9	0.490	H-4→L(33%)			H-1→L+2(24%)			H-4→L(14%)
		H-2→L+1(34%)	741.3	0.913	H→L(85%)			H-2→L+2(29%)			H-4→L(16%)	390.4	0.076	H-3→L+1(71%)
445.5	0.452	H→L+2(28%)	604.7	0.298	H-1→L(80%)			H-1→L+3(18%)			H-4→L+2(14%)	386.8	0.019	H-3→L+2(68%)
		H-3→L(14%)	583.5	0.025	H→L+1(58%)	404.7	0.322	H-3→L+1(70%)	382.2	0.015	H-7→L(55%)			H→L+3(16%)
		H-1→L+1(13%)			H→L(12%)	403.3	0.074	H-7→L(41%)			H-8→L(34%)	360.5	0.124	H-4→L+1(47%)
		H-2→L+1(13%)			H→L+3(11%)			H-8→L(21%)	378.6	0.684	H-4→L+1(71%)	358.2	0.014	H-4→L+2(16%)
		H-4→L(11%)			H-2→L+2(10%)			H-4→L(11%)			H-2→L+2(17%)	354.8	0.016	H-5→L+1(11%)

[a] Only oscillator strength $f > 0.01$ and orbital percentage > 10% are reported, where H = HOMO and L = LUMO.

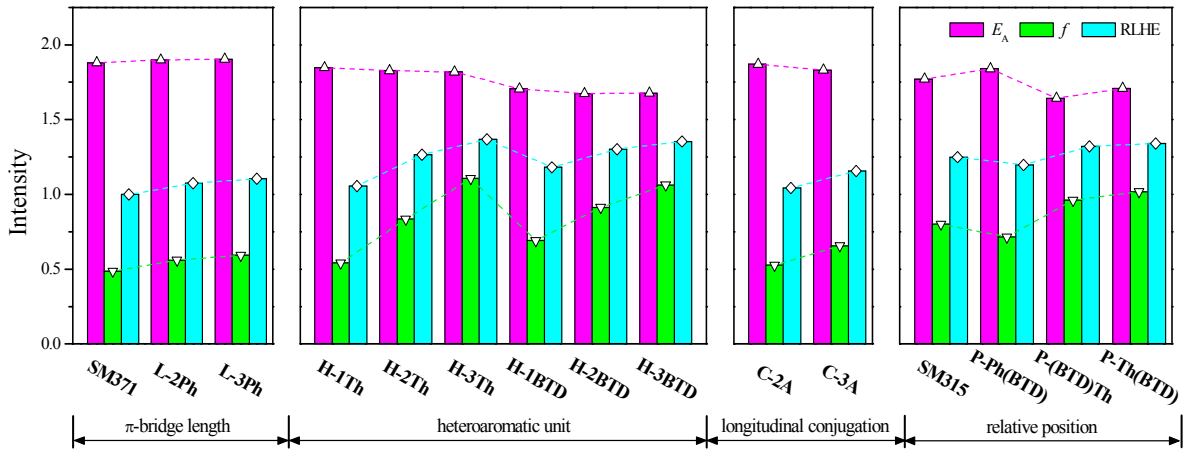

Fig. 5 The comparison in the lowest vertical excitation energies (E_A), oscillator strengths (f), and relative LHE (RLHE) of all porphyrin sensitizers calculated in THF solution. **All energies are in eV.**

transitions via HOMO → LUMO/LUMO+1 with f = 1.062, also exhibiting long-range LLET characteristics. Noticeably, the absorption strength of the first vertical excitations of **H-1Th** – **H-3Th** and **H-1BTD** – **H-3BTD** increases by a maximum of 38% and a minimum of 11% relative to those of **SM315** and **SM371**, respectively. This increase would be of great help to the performance of porphyrin-sensitized DSSCs [73]. In short, increasing Th/BTD number can weaken the B band but strengthen the Q band significantly.

Extending the longitudinal π-conjugation by substituting naphthalene/anthracene for Ph weakens but broadens the B band,while slightly strengthens and redshifts the Q band of **C-2A** and **C-3A** relative to that of **SM371**, as shown in Figs. 4a and 4c. At ~448 nm, the B band of **C-2A** mainly originates from the mixed transitions via HOMO/HOMO-1/HOMO-2 to LUMO/LUMO+1/LUMO+2 at 456.1 nm (f = 1.472), HOMO-1/HOMO-2/HOMO-3 to LUMO/LUMO+1 at 424.2 nm (f = 0.741), and HOMO/HOMO-2/HOMO-7 to LUMO/LUMO+1/LUMO+2 at 421.9 nm (f = 0.405). Among these transitions, those to LUMO/LUMO+2 are favorable for the charge separation. For **C-3A**, a wide B band is detected that includes two peaks at ~377 and ~498 nm, in which most of the transitions at 378.6 and 508.1 nm are unfavorable whereas those at 371.2 and 500.2 nm are effective, as indicated in Table S2. (ESI†) Noticeably, 90% of the transitions of the first vertical excitation of acene-bridged sensitizers occur from the HOMO to the LUMO with strong absorption intensity, including the transitions at 662.8 nm with f = 0.527 for **C-2A** and at 677.0 nm with f = 0.657 for **C-3A**. According to the molecular orbital analysis, these transitions are favorable for the efficient charge separation and electron injection.

Repositioning Ph and BTD from **SM315** to **P-Ph(BTD)** shortens spectral range but enhances the B band intensity significantly. Replacing Ph with Th induces the Q band redshifted but weankens both B and Q band intensities, as depicted in Fig. 4d. When Ph/Th is distanced from the carboxylic acid, the peaks move from 418.4/699.3 nm of **SM315** to 427.4/675.7 nm of **P-Ph(BTD)** and from 418.4/729.9 nm of **P-(BTD)Th** to 432.9/724.6 nm of **P-Th(BTD)**. This scenario agrees well with the energy gap analysis. For **SM315**, **P-Ph(BTD)**, **P-(BTD)Th**, and **P-Th(BTD)**, the first vertical excitations display LLET characteristics via over 80% HOMO → LUMO transition with $f \geq 0.715$, thus guaranteeing the spectral performance at the near-infrared region. For the B band, more effective electron transitions occur when Ph/Th is distanced from the carboxylic acid. For instance, only 33% effective transitions to the LUMO occur at 429.6 nm with f = 0.992 for **SM315**, while 27% effective transitions at 432.2 nm with f = 1.859, 38% transitions at 432.2 nm with f = 0.952 and 95% transitions at 402.2 nm with f = 0.126 for **P-Ph(BTD)**. A similar case appears when going from **P-(BTD)Th** to **P-Th(BTD)**.

3.5 Light-harvesting efficiency (LHE)

With the effect of functionalized π-bridge linkers, the designed porphyrin sensitizers exhibit excellent properties in electronic structure, electron excitation, and absorption spectra relative to **SM315** and **SM371**. As an indicator of incident photo-to-electron conversion efficiency, LHE characterizes the capability of sensitizers in harvesting light. Sensitizers with high LHE ensure the better photocurrent response. The LHE can be approximated as [74]

$$\mathrm{LHE} = 1 - 10^{-A} = 1 - 10^{-f} \quad (4)$$

where A(f) is the absorption (oscillator strength) of the sensitizer associated with the lowest vertical excitation energy (E_A).

The comparison in the lowest vertical excitation energies (E_A), oscillator strengths (f), and relative LHE (RLHE) of all porphyrin sensitizers are shown in Fig. 5. The values of HOMO and LUMO energies, HOMO-LUMO gaps, the lowest vertical excitation energies (E_A), oscillator strengths (f), and relative LHE (RLHE) are listed in Table S3 (ESI†). The reference sensitizer **SM371** has achieved remarkable performance with only a Ph-bridged linker [40]; thus, the LHE of the newly designed sensitizers is evaluated through comparison with **SM371**, that is, $\mathrm{RLHE} = \mathrm{LHE}_{\mathbf{Sensitizers}}/\mathrm{LHE}_{\mathbf{SM371}}$. Seen from Fig. 5 and Table S3, the increase in π-bridge length, the extension of longitudinal conjugation, and the introduction of heteroaromatics contribute to the improvement of light-harvesting capability and enhance LHE by at least 4.3%. This is related to the oscillator strengths enhanced with the functionalization on **SM371**,

Table 2. The calculated optical and electronic properties as well as IET parameters of porphyrin sensitizers.

Sensitizers	λ (nm)	q^{ET} [a] (e)	d^{ET} [b] (Å)	H [c] (Å)	t [d] (Å)	V_{ab} (cm^{-1})	λ_v (eV)	k_{ET} (fs^{-1})
SM315	700.2	0.899	7.798	7.213	0.585	3164	0.189	0.94
P-Ph(BTD)	673.9	0.975	10.229	8.220	2.009	3528	0.244	0.61
P-(BTD)Th	735.4	0.910	8.482	7.371	1.111	4778	0.173	2.62
P-Th(BTD)	725.4	0.936	9.774	8.017	1.757	2872	0.300	2.09
SM371	659.5	0.919	5.259	5.974	-0.715	4280	0.149	2.86
L-2Ph	399.6	0.826	10.828	8.460	2.368	997	0.135	0.19
L-3Ph	355.3	0.758	7.263	8.450	-1.187	1008	0.120	0.24
H-1Th	671.2	1.054	5.055	6.589	-1.534	3176	0.162	1.33
H-2Th	678.7	1.094	5.176	7.753	-2.577	6183	0.155	5.56
H-3Th	681.7	1.322	4.019	8.166	-4.147	6614	0.146	7.14
C-2A	662.8	0.913	5.495	6.150	-0.655	5492	0.192	2.76
C-3A	677.0	1.404	3.710	7.871	-4.161	5844	0.221	2.18
H-1BTD	727.3	1.513	5.207	7.909	-2.702	4341	0.186	1.85
H-2BTD	741.3	0.974	9.689	7.826	1.863	4158	0.232	0.97
H-3BTD	739.4	1.003	11.041	8.635	2.406	4178	0.247	0.82

[a] q^{ET} is the transferred charge which can be obtained by integrating over all space $\rho_+(r)$ or $\rho_-(r)$. For one electron excitation, q can be assumed between 0 and 1.
[b] d^{ET} defines the spatial distance between the two barycentres of the density enhancement ($\rho_+(r) = \Delta\rho(r)$, if $\Delta\rho < 0$) and density depletion ($\rho_-(r) = \Delta\rho(r)$, if $\Delta\rho > 0$) distribution upon excitation.
[c] H is the half of the sum of the centroids axis along electron transfer direction.
[d] t represents the difference between d^{ET} and H: $t = d^{ET} - H$, for $H \geq d^{ET}$, an overlap between the density increment and depletion regions is thus foresaw.

as reflected by the f value ranging from 0.527 to 1.106 in comparison with 0.487 for **SM371**. The greater the increasment of π-bridge length in the π-bridge linker (**SM371** → **L-2Ph**, **L-3Ph**), the greater the LHE, as reflected by the increase in RLHE from 1.000 to 1.074 and 1.105. A similar case appears for the extension of the longitudinal conjugation (**SM371** → **C-2A**, **C-3A**) in the π-bridge linker, giving rise to the RLHE from 1.000 to 1.043 and 1.157. Comparatively, the introduction of heteroaromatics, including the $_{Ph(BTD)}$/LHE_{SM315} = 0.958, and further introducting Th into **P-(BTD)Th** and **P-Th(BTD)** enhances RLHE to $LHE_{P-(BTD)Th}/LHE_{SM315}$ = 1.058 and $LHE_{P-Th(BTD)}/LHE_{P-Ph(BTD)}$ = 1.120. This findings also highlights the positive effect of heteroaromatic groups on the light-harvesting performance.

3.6 Intramolecular electron transfer (IET)

Usually, the favorable photo-induced IET properties would enhance the efficiency of charge separation and electron injection for sensitizers with D-π-A structure [75]. Herein, the IET parameters, including the IET rate (k_{ET}), transferred charge (q^{ET}), electron transfer distance (d^{ET}), H, and t at specific photo-excitation wavelength (λ) are analyzed, as shown in Table 2. More calculation details can be founded in previous studies [70, 76-81].

For the Ph-bridged sensitizers, the q^{ET} decreases with the increase in the π-bridge length, following the sequence of 0.919 e (**SM371**) < 0.826 e (**L-2Ph**) < 0.758 e (**L-3Ph**). The donor-to-acceptor IET rates k_{ET} of **L-2Ph** and **L-3Ph** are calculated to be 0.19 and 0.24 fs^{-1}, an order of magnitude smaller than 2.86 fs^{-1} for **SM371**. This result is attributed to the sharp decrease in the electronic coupling between the initial and final states from 4280 cm^{-1} for **SM371** to 997 and 1008 cm^{-1} for **L-2Ph** and **L-3Ph**, respectively. Although the increase in the π-bridge length has a negative effect on q^{ET} and k_{ET}, Th (**SM371** → **H-1Th** – **H-3Th**) and BTD (**SM371** → **H-1BTD** – **H-3BTD**) groups in π-bridge linkers, significantly boosts RLHE to LHE_{H-3Th}/LHE_{SM371} = 1.367 and LHE_{H-3BTD}/LHE_{SM371} = 1.355. The redshifted spectra together with the sharply enhanced f values of **H-1Th** – **H-3Th** and **H-1BTD** – **H-3BTD** highlight the significant roles of heteroaromatic group for sensitizers in the light harvesting capability at the long wavelength region. Repositioning the Ph group from **SM315** to **P-Ph(BTD)** decreases RLHE to LHE_{P-}. the large d^{ET} of 10.828 Å and t of 2.368 Å indicate that **L-2Ph** is in a more effective charge-separated state.

Introducing electron-rich Th and electron-deficient BTD significantly increases the amount of q^{ET} by 0.135 – 0.403 e for **H-1Th** – **H-3Th** and 0.055 – 0.594 e for **H-1BTD** – **H-3BTD** in comparison with 0.919 e for **SM371**, as indicated in Table 2. The t value follows the sequence of -4.147 Å (**H-3Th**) < -2.577 Å (**H-2Th**) < -1.534 Å (**H-1Th**), suggesting that introducing more electron-rich units into the bridge linker would increase orbital overlap as well. Comparatively, the t value follows the sequence of -2.702 Å (**H-1BTD**) < 1.863 Å (**H-2BTD**) < 2.406 Å (**H-3BTD**), indicating that introducing more electron-deficient units into the bridge linker would reduce orbital overlap. Interestingly, the increase in π-bridge length from **H-1Th** to **H-2Th** and **H-3Th** accelerates IET from 1.33 to 5.56 and 7.14 fs^{-1}; however, the IET rate of the **BTD**-bridged sensitizers decreases from 1.85 fs^{-1} (**H-1BTD**) to 0.97 fs^{-1} (**H-2BTD**) and 0.82 fs^{-1} (**H-3BTD**). In short, introducing more electron-rich units into the bridge linker enhances IET rate but increase orbital overlap. By contrast, integrating more electron-deficient units lowers IET rate but reduces orbital overlap as well. Nonetheless, both electron-rich and electron-deficient units can promote the amount of transferred electrons.

With the extension of longitudinal conjugation, an electron transfer of 1.404 e over 3.710 Å is observed for **C-3A** at a rate of

2.18 fs^{-1}, whereas over 1.500 Å shorter in d^{ET} with a slightly lower rate than for **SM371** with d^{ET} = 5.259 Å and k_{ET} = 2.86 fs^{-1}, and **C-2A** with d^{ET} = 5.495 Å and k_{ET} = 2.76 fs^{-1}. The t = -4.166 Å for **C-3A** implies a significant orbital overlap between electron-donating and electron-accepting regions. As a result, the IET performance of **SM371** and **C-2A** is expected to be superior to that of **C-3A**, as in the case of **YD11**–**YD13** porphyrin-sensitized solar cells [16].

Inserting Ph or Th between the Zn-porphyrin core and BTD group reduce IET rate from 0.94 fs^{-1} in **SM315** to 0.61 fs^{-1} in **P-Ph(BTD)** and from 2.62 fs^{-1} in **P-(BTD)Th** to 2.09 fs^{-1} in **P-Th(BTD)**, as shown in Table 2. **P-Ph(BTD)** and **P-Th(BTD)** are also superior to **SM315** and **P-(BTD)Th** in that the formers exhibit higher q^{ET} values of 0.975 and 0.936 e, d^{ET} values of 10.229 and 9.774 Å, and t values of 2.009 and 1.757 Å. It indicates that the IET rate and charge separation efficiency can be controlled by suitably adjusting the relative position of the units embedded between the Zn-porphyrin core and the anchoring group.

To sum up, keeping a good balance among the electronic structure, electron excitation and spectra, LHE, and photo-induced IET properties would be of great help to the overall performance of porphyrin sensitizers. By adjusting the π-bridge length, heteroaromatic unit, longitudinal conjugation, and relative position of functionalized groups, porphyrin sensitizers can be designed to improve the light-harvesting capability, charge separation and electron injection efficiency, and the matching degree with semiconductor and electrolyte. As a result, continuous progresses in sensitizers can be achieved and excellent photon-to-electron conversion efficiencies can be envisaged for DSSCs, as sensitizers **SM315** and **SM371**.

4. Conclusion

A series of porphyrin sensitizers have been systematically investigated to evaluate the effects of the functionalized π-bridge on DSSCs performance using DFT and TD-DFT approach in THF solution. The main points are summarized as follows:

(1) The increase in π-bridge length by adding Ph group keeps the electron distribution of LUMO away from the anchoring group, decreases the spectral coverage and the proportion of effective electron excitation, and therefore sharply reduces the donor-to-acceptor IET and the photon-to-electron conversion at the long wavelength region.

(2) The introduction of heteroaromatics in the π-bridge stabilizes LUMO levels and thus reduces energy gaps, and improves the light-harvesting capability significantly. Introducing electron-rich units in π-bridge accelerates the IET process but increases the orbital overlap between donor and acceptor regions, while electron-deficient units enhances the spectral response to the near-infrared light and leads to long-range IET with low orbital overlap. Both electron-rich and electron-deficient heteroaromatic units can promote the amount of transferred electrons.

(3) The extension of longitudinal π-conjugation broadens the B band, and slightly strengthens and redshifts the Q band. However, the short transfer distance, slow IET rate, and high orbital overlap indicate the unfavorable IET characteristics and photo-to-electron conversion performance.

(4) Repositioning Ph/Th group away from carboxylic acid enlarges the energy gap and shortens the spectral coverage slightly, but yields more effective donor-to-acceptor electron transitions. The favorable long-range IET processes with more electron, longer distance, lower orbital overlap and moderate transfer rate are allowed when the heteroaromatic BTD group is positioned near carboxylic acid.

Acknowledgements

This work was supported by NSFC (21303266), Promotive Research Fund for Excellent Young and Middle-aged Scientists of Shandong Province (BS2013CL031), PetroChina Innovation Foundation (2013D-5006-0406), and the Fundamental Research Funds for the Central Universities (15CX08009A). We also thank Key Laboratory of Artificial Structures and Quantum Control for the supporting.

Notes and references

1 B. O'Regan and M. Grätzel, *Nature*, 1991, **353**, 737-740.
2 A. Kay and M. Grätzel, *J. Phys. Chem.*, 1993, **97**, 6272-6277.
3 M. Grätzel, *Acc. Chem. Res.*, 2009, **42**, 1788-1798.
4 Q. J. Yu, Y. H. Wang, Z. H. Yi, N. N. Zu, J. Zhang, M. Zhang and P. Wang, *ACS Nano*, 2010, **4**, 6032-6038.
5 A. Hagfeldt, G. Boschloo, L. Sun, L. Kloo and H. Pettersson, *Chem. Rev.*, 2010, **110**, 6595-6663.
6 M. Sandroni, L. Favereau, A. Planchat, H. Akdas-Kilig, N. Szuwarski, Y. Pellegrin, E. Blart, H. Le Bozec, M. Boujtita and F. Odobel, *J. Mater. Chem. A*, 2014, **2**, 9944-9947.
7 X. Q. Lu, S. X. Wei, C.-M. L. Wu, S. R. Li and W. Y. Guo, *J. Phys. Chem. C*, 2011, **115**, 3753-3761.
8 A. Yella, H.-W. Lee, H. N. Tsao, C. Y. Yi, A. K. Chandiran, M. K. Nazeeruddin, E. W.-G. Diau, C.-Y. Yeh, S. M. Zakeeruddin and M. Grätzel, *Science*, 2011, **334**, 629-634.
9 L.-L. Li and E. W.-G. Diau, *Chem. Soc. Rev.*, 2013, **42**, 291-304.
10 A. Yella, C.-L. Mai, S. M. Zakeeruddin, S.-N. Chang, C.-H. Hsieh, C.-Y. Yeh and M. Grätzel, *Angew. Chem.*, 2014, **126**, 3017-3021.
11 A. Mishra, M. K. R. Fischer and P. Bäuerle, *Angew. Chem. Int. Ed*, 2009, **48**, 2474-2499.
12 J. F. Lu, S. S. Liu, H. Li, Y. Shen, J. Xu, Y. B. Cheng and M. K. Wang, *J. Mater. Chem. A*, 2014, **2**, 17495-17501.
13 K. P. Guo, K. Y. Yan, X. Q. Lu, Y. C. Qiu, Z. K. Liu, J. W. Sun, F. Yan, W. Y. Guo and S. H. Yang, *Org. Lett.*, 2012, **14**, 2214-2217.
14 X. F. Shi, X. Q. Lu, Y. Shao, S. X. Wei, Q. Zhu, D. L. Jin, Z. G. Deng and W. Y. Guo, *Sci. Adv. Mater.*, 2014, **6**, 2595-2602.
15 P. Gao, Y. J. Kim, J.-H. Yum, T. W. Holcombe, M. K. Nazeeruddin and M. Grätzel, *J. Mater. Chem. A*, 2013, **1**, 5535-5544.
16 H. P. Lu, C. L. Mai, C. Y. Tsia, S. J. Hsu, C. P. Hsieh, C. L. Chiu, C. Y. Yeh and E. W. G. Diau, *Phys. Chem. Chem. Phys.*, 2009, **11**, 10270-10274.
17 C. Y. Lin, Y. C. Wang, S. J. Hsu, C. F. Lo and E. W. G. Diau, *J. Phys. Chem. C*, 2009, **114**, 687-693.
18 C. F. A. Negre, R. L. Milot, L. A. Martini, W. Ding, R. H. Crabtree, C. A. Schmuttenmaer and V. S. Batista, *J. Phys. Chem. C*, 2013, **117**, 24462-24470.
19 C. H. Wu, M. C. Chen, P. C. Su, H. H. Kuo, C. L. Wang, C. Y. Lu, C. H. Tsai, C. C. Wu and C. Y. Lin, *J. Mater. Chem. A*, 2014, **2**, 991-999.
20 K. B. Ornso, J. M. Garcia-Lastra and K. S. Thygesen, *Phys. Chem. Chem. Phys.*, 2013, **15**, 19478-19486.
21 M. K. Panda, K. Ladomenou and A. G. Coutsolelos, *Coord. Chem. Rev.*, 2012, **256**, 2601-2627.

22 H. P. Lu, C. Y. Tsai, W. N. Yen, C. P. Hsieh, C. W. Lee, C. Y. Yeh and E. W. G. Diau, *J. Phys. Chem. C*, 2009, **113**, 20990-20997.
23 C. H. Wu, T. Y. Pan, S. H. Hong, C. L. Wang, H. H. Kuo, Y. Y. Chu, E. W. G. Diau and C. Y. Lin, *Chem. Commun.*, 2012, **48**, 4329-4331.
24 C. L. Wang, Y. C. Chang, C. M. Lan, C. F. Lo, E. Wei-Guang Diau and C. Y. Lin, *Energ. Environ. Sci.*, 2011, **4**, 1788-1795.
25 Y. C. Chang, C. L. Wang, T. Y. Pan, S. H. Hong, C. M. Lan, H. H. Kuo, C. F. Lo, H. Y. Hsu, C. Y. Lin and E. W. G. Diau, *Chem. Commun.*, 2011, **47**, 8910-8912.
26 C. L. Wang, C. M. Lan, S. H. Hong, Y. F. Wang, T. Y. Pan, C. W. Chang, H. H. Kuo, M. Y. Kuo, E. W. G. Diau and C. Y. Lin, *Energ. Environ. Sci.*, 2012, **5**, 6933-6940.
27 W. M. Campbell, K. W. Jolley, P. Wagner, K. Wagner, P. J. Walsh, K. C. Gordon, L. Schmidt-Mende, M. K. Nazeeruddin, Q. Wang, M. Grätzel and D. L. Officer, *J. Phys. Chem. C*, 2007, **111**, 11760-11762.
28 C. Yi, F. Giordano, N.-L. Cevey-Ha, H. N. Tsao, S. M. Zakeeruddin and M. Grätzel, *ChemSusChem*, 2014, **7**, 1107-1113.
29 M. D. Zhang, Z. Y. Zhang, Z. Q. Bao, Z. M. Ju, X. Y. Wang, H. G. Zheng, J. Ma and X. F. Zhou, *J. Mater. Chem. A*, 2014, **2**, 14883-14889.
30 M. P. Balanay and D. H. Kim, *Physical Chemistry Chemical Physics*, 2008, **10**, 5121-5127.
31 C. F. Lo, L. Luo, E. W. G. Diau, I. J. Chang and C. Y. Lin, *Chem. Commun.*, 2006, 1430-1432.
32 C. Y. Lin, C. F. Lo, L. Luo, H. P. Lu, C. S. Hung and E. W. G. Diau, *J. Phys. Chem. C*, 2009, **113**, 755-764.
33 M. K. Nazeeruddin, R. Humphry-Baker, D. L. Officer, W. M. Campbell, A. K. Burrell and M. Grätzel, *Langmuir*, 2004, **20**, 6514-6517.
34 Q. Wang, W. M. Campbell, E. E. Bonfantani, K. W. Jolley, D. L. Officer, P. J. Walsh, K. Gordon, R. Humphry-Baker, M. K. Nazeeruddin and M. Grätzel, *J. Phys. Chem. B*, 2005, **109**, 15397-15409.
35 W. P. Zhou, Z. C. Cao, S. H. Jiang, H. Y. Huang, L. J. Deng, Y. J. Liu, P. Shen, B. Zhao, S. T. Tan and X. X. Zhang, *Org. Electron.*, 2012, **13**, 560-569.
36 S. Mathew, H. Iijima, Y. Toude, T. Umeyama, Y. Matano, S. Ito, N. V. Tkachenko, H. Lemmetyinen and H. Imahori, *J. Phys. Chem. C*, 2011, **115**, 14415-14424.
37 L. Favereau, J. Warnan, F. B. Anne, Y. Pellegrin, E. Blart, D. Jacquemin and F. Odobel, *J. Mater. Chem. A*, 2013, **1**, 7572-7575.
38 Y. J. Liu, N. Xiang, X. M. Feng, P. Shen, W. P. Zhou, C. Weng, B. Zhao and S. T. Tan, *Chem. Commun.*, 2009, 2499-2501.
39 T. Higashino and H. Imahori, *Dalton Trans.*, 2015, **44**, 448-463.
40 S. Mathew, A. Yella, P. Gao, R. Humphry-Baker, F. E. CurchodBasile, N. Ashari-Astani, I. Tavernelli, U. Rothlisberger, K. NazeeruddinMd and M. Grätzel, *Nat. Chem.*, 2014, **6**, 242-247.
41 C. Lee, W. Yang and R. G. Parr, *Phys. Rev. B*, 1988, **37**, 785-789.
42 A. D. Becke, *J. Chem. Phys.*, 1993, **98**, 1372-1377.
43 G. A. Petersson, T. G. Tensfeldt and J. A. Montgomery, *J. Chem. Phys.*, 1991, **94**, 6091-6101.
44 T. Yanai, D. P. Tew and N. C. Handy, *Chem. Phys. Lett.*, 2004, **393**, 51-57.
45 S. S. Zhang, Z. X. Qu, P. Tao, B. Brooks, Y. H. Shao, X. Y. Chen and C. G. Liu, *J. Phys. Chem. C*, 2012, **116**, 12434-12442.
46 N. Santhanamoorthi, C.-M. Lo and J.-C. Jiang, *J. Phys. Chem. Lett.*, 2013, **4**, 524-530.
47 M. Ernzerhof and G. E. Scuseria, *J. Chem. Phys.*, 1999, **110**, 5029-5036.
48 C. Adamo and V. Barone, *J. Chem. Phys.*, 1999, **110**, 6158-6170.
49 Y. Zhao and D. Truhlar, *Theor. Chem. Acc.*, 2008, **120**, 215-241.
50 A. Filippo De, F. Simona and S. Annabella, *Nanotechnology*, 2008, **19**, 424002.
51 R. E. Stratmann, G. E. Scuseria and M. J. Frisch, *J. Chem. Phys.*, 1998, **109**, 8218-8224.
52 G. Scalmani, M. J. Frisch, B. Mennucci, J. Tomasi, R. Cammi and V. Barone, *J. Chem. Phys.*, 2006, **124**, 094107.
53 M. Cossi and V. Barone, *J. Chem. Phys.*, 2001, **115**, 4708-4717.
54 S. Miertuš, E. Scrocco and J. Tomasi, *Chem. Phys.*, 1981, **55**, 117-129.
55 M. Cossi, V. Barone, R. Cammi and J. Tomasi, *Chem. Phys. Lett.*, 1996, **255**, 327-335.
56 V. Barone and M. Cossi, *J. Phys. Chem. A*, 1998, **102**, 1995-2001.
57 M. J. Frisch, G. W. Trucks, H. B. Schlegel, G. E. Scuseria, M. A. Robb, J. R. Cheeseman, G. Scalmani, V. Barone, B. Mennucci, G. A. Petersson, H. Nakatsuji, M. Caricato, X. Li, H. P. Hratchian, A. F. Izmaylov, J. Bloino, G. Zheng, J. L. Sonnenberg, M. Hada, M. Ehara, K. Toyota, R. Fukuda, J. Hasegawa, M. Ishida, T. Nakajima, Y. Honda, O. Kitao, H. Nakai, T. Vreven, J. A. Montgomery Jr., J. E. Peralta, F. Ogliaro, M. Bearpark, J. J. Heyd, E. Brothers, K. N. Kudin, V. N. Staroverov, R. Kobayashi, J. Normand, K. Raghavachari, A. Rendell, J. C. Burant, S. S. Iyengar, J. Tomasi, M. Cossi, N. Rega, J. M. Millam, M. Klene, J. E. Knox, J. B. Cross, V. Bakken, C. Adamo, J. Jaramillo, R. Gomperts, R. E. Stratmann, O. Yazyev, A. J. Austin, R. Cammi, C. Pomelli, J. W. Ochterski, R. L. Martin, K. Morokuma, V. G. Zakrzewski, G. A. Voth, P. Salvador, J. J. Dannenberg, S. Dapprich, A. D. Daniels, Ö. Farkas, J. B. Foresman, J. V. Ortiz, J. Cioslowski and D. J. Fox, *Wallingford, CT*, 2009.
58 J. H. Yang, W. W. Zhang, Y. B. Si and Y. Zhao, *J. Phys. Chem. B*, 2012, **116**, 14126-14135.
59 A. Farazdel, M. Dupuis, E. Clementi and A. Aviram, *J. Am. Chem. Soc.*, 1990, **112**, 4206-4214.
60 W. W. Zhang, W. J. Zhu, W. Z. Liang, Y. Zhao and S. F. Nelsen, *J. Phys. Chem. B*, 2008, **112**, 11079-11086.
61 V. Vaissier, P. Barnes, J. Kirkpatrick and J. Nelson, *Phys. Chem. Chem. Phys.*, 2013, **15**, 4804-4814.
62 S. F. Nelsen, S. C. Blackstock and Y. Kim, *J. Am. Chem. Soc.*, 1987, **109**, 677-682.
63 S. F. Nelsen, *J. Am. Chem. Soc.*, 1996, **118**, 2047-2058.
64 J.-L. Brédas, D. Beljonne, V. Coropceanu and J. Cornil, *Chem. Rev.*, 2004, **104**, 4971-5004.
65 P. Song, Y. Z. Li, F. C. Ma, T. Pullerits and M. T. Sun, *J. Phys. Chem. C*, 2013, **117**, 15879-15889.
66 Q. Wu and T. Van Voorhis, *J. Phys. Chem. A*, 2006, **110**, 9212-9218.
67 M. Rossi and K. Sohlberg, *J. Phys. Chem. C*, 2010, **114**, 12173-12189.
68 C. Lee, R. Waterland and K. Sohlberg, *J. Chem. Theory Comput.*, 2011, **7**, 2556-2567.
69 H. M. Qin, X. X. Zhong, Y. B. Si, W. W. Zhang and Y. Zhao, *J. Phys. Chem. A*, 2011, **115**, 3116-3121.
70 Y. Shao, X. Q. Lu, K. Li, Z. G. Zhao, X. F. Shi, D. L. Jin, H. Y. Zhu, G. W. Yang and W. Y. Guo, *Mater. Chem. Phys.*, 2015, **162**, 6-10.
71 K. Pettersson, A. Kyrychenko, E. Rönnow, T. Ljungdahl, J. Mårtensson and B. Albinsson, *J. Phys. Chem. A*, 2005, **110**, 310-318.
72 M. Y. Guo, M. Li, Y. L. Dai, W. Shen, J. D. Peng, C. Y. Zhu, S. H. Lin and R. X. He, *RSC Adv.*, 2013, **3**, 17515-17526.
73 C.-Y. Chen, M. Wang, J.-Y. Li, N. Pootrakulchote, L. Alibabaei, C.-h. Ngoc-le, J.-D. Decoppet, J.-H. Tsai, C. Grätzel, C.-G. Wu, S. M. Zakeeruddin and M. Grätzel, *ACS Nano*, 2009, **3**, 3103-3109.

74 H. S. Nalwa, *Handbook of Advanced Electronic and Photonic Materials and Devices: Conducting polymers*, Academic Press, 2001.
75 W. Li, F.-Q. Bai, J. Chen, J. Wang and H. X. Zhang, *J. Power Sources*, 2015, **275**, 207-216.
76 T. Le Bahers, C. Adamo and I. Ciofini, *J. Chem. Theory Comput.*, 2011, **7**, 2498-2506.
77 D. Jacquemin, T. L. Bahers, C. Adamo and I. Ciofini, *Phys. Chem. Chem. Phys.*, 2012, **14**, 5383-5388.
78 I. Ciofini, T. Le Bahers, C. Adamo, F. Odobel and D. Jacquemin, *J. Phys. Chem. C*, 2012, **116**, 11946-11955.
79 R. A. Marcus, *Annu. Rev. Phys. Chem.*, 1964, **15**, 155-196.
80 R. A. M. and N. Sutin., *Biochim. Biophys. Acta*, 1985, **811**, 265-322.
81 R. A. Marcus, *J. Chem. Phys.*, 1956, **24**, 966-978.

GRAPHIC ABSTRACT:

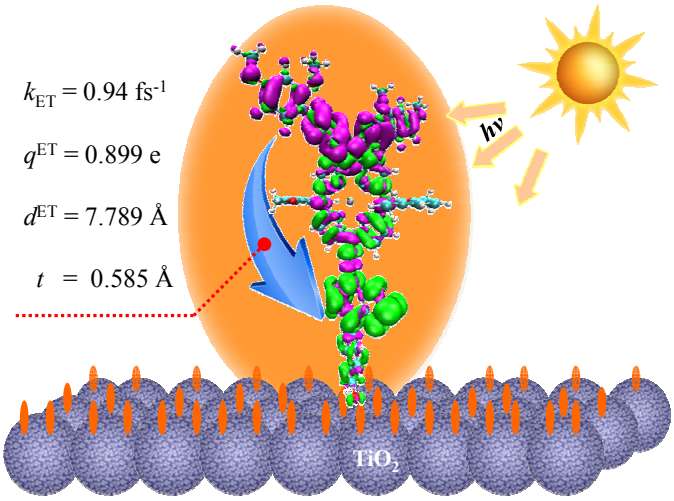

The effects of π-bridge length, heteroaromatic unit, longitudinal conjugation, and relative position of functionalized groups on the optical and electrical properties of porphyrin sensitizers are elucidated by analyzing the geometry, electronic structure, electron excitation, spectrum, photo-induced intramolecular electron transfer (IET), and light-harvesting efficiency (LHE).